doi:10.1038/nature10633

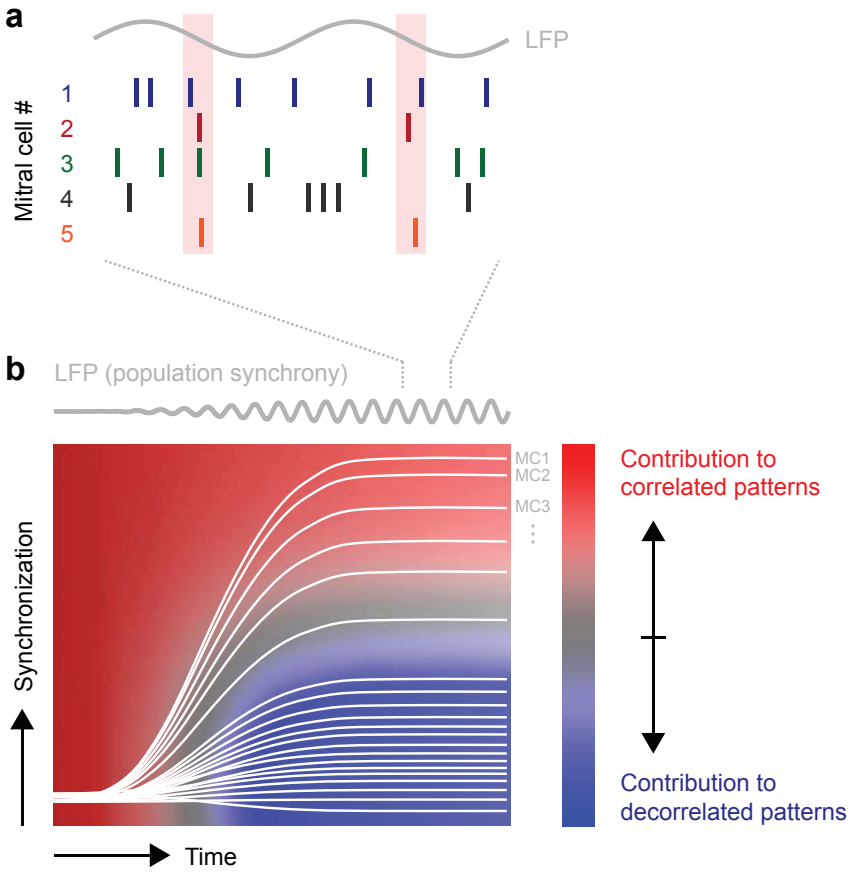

Supplementary Figure 1 | Schematic illustration of multiplexed odor representations in the zebrafish OB. **a**, During the oscillatory phase of an odor response, some MCs phase-lock to the LFP oscillation (e.g., MC 2 and 5) while others do not, even though they often fire at relatively high rates (e.g., MC 1 and 3). As a consequence, action potentials of specific MC subsets are synchronized at the oscillation frequency of approximately 20 Hz (red shading), but the majority of action potentials shows no obvious oscillatory synchronization. Patterns of synchronized (phase-locked) action potentials across MCs are highly correlated in response to chemically similar odors. Hence, synchronized spike patterns are informative about molecular categories of odors but do not efficiently encode precise odor identity. Patterns of non-synchronized action potentials, in contrast, become decorrelated in response to similar odors and informative about precise odor identity. MC activity patterns therefore simultaneously convey information about complementary stimulus features (multiplexing)[1]. **b**, Development of multiplexed representations during an odor response. White lines schematically show the synchronization of individual MC responses as a function of time. Background color represents the contribution of MCs to correlated or decorrelated representations of similar odors as a function of time and synchronization. Initially, MC response patterns are not obviously synchronized and correlated. Subsequently, oscillatory synchronization emerges and activity patterns are reorganized, resulting in an overall decorrelation of patterns evoked by similar odors. The majority of MCs does not strongly phase-lock to the oscillation and contributes to decorrelated activity patterns. However, an odor-dependent minority of MCs phase-lock to the oscillation and give rise to correlated activity patterns. Decorrelated activity patterns at later times of the odor response and are therefore carried specifically by MCs that do not strongly phase-lock to the oscillation. Information about precise odor identity would thus be extracted most efficiently from late activity patterns across non-synchronized MCs. However, extracting this information may be complicated by synchronized MCs because even a small number of synchronized inputs can have a strong impact on target neurons.

1 Friedrich, R. W., Habermann, C. J. & Laurent, G. Multiplexing using synchrony in the zebrafish olfactory bulb. *Nature Neurosci.* **7**, 862-871 (2004).

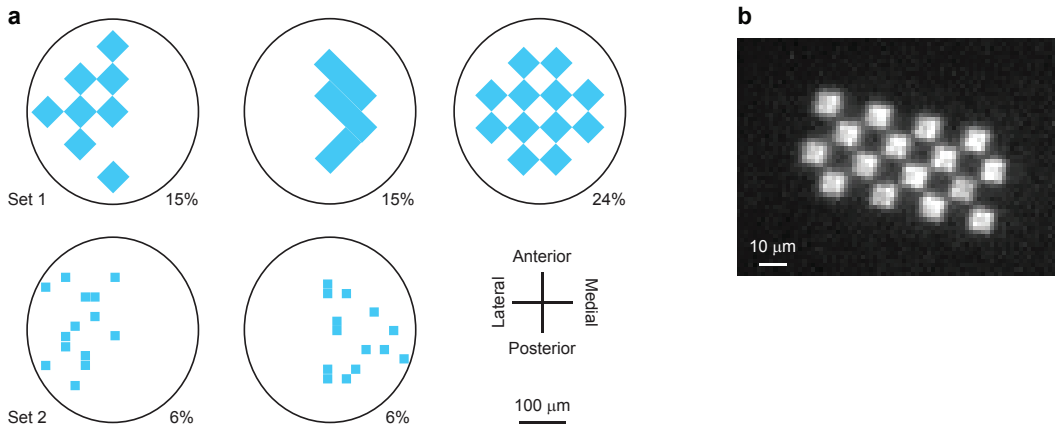

Supplementary Figure 2 | Optical stimulus patterns. **a**, Examples of optical stimulus patterns from set 1 (top) and set 2 (bottom). Oval outlines approximate boundary of the OB. Percentages report the approximate fraction of the OB cross section that is covered by active squares in each pattern. **b**, Fluorescence image of a thin film of fluorescein illuminated with a blue checkerboard pattern from the DMD. Each square is 7 x 7 μm^2 and can be clearly resolved.

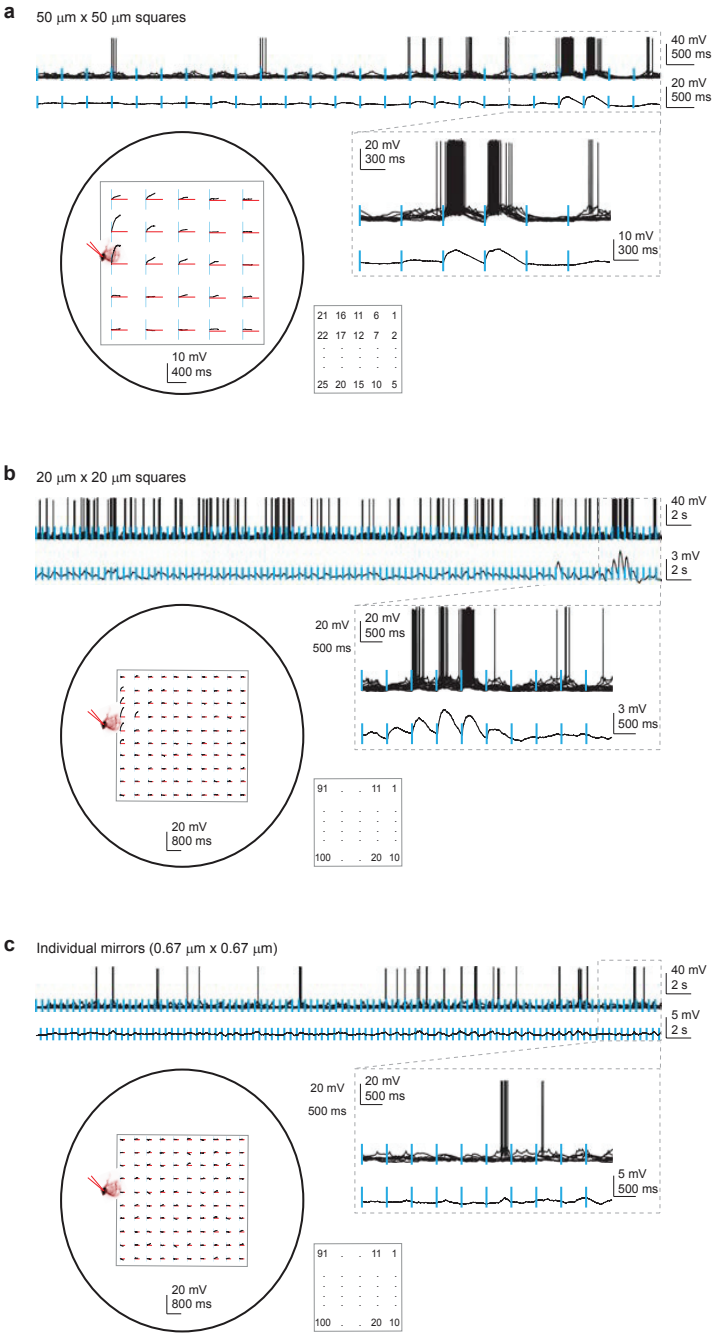

Supplementary Figure 3 | Responses to optical stimulation with individual squares. **a**, Individual squares from stimulus set 1 (50 x 50 µm^2) were switched on successively for 5 ms at a rate of 2 Hz (blue ticks) while recording from a MC in a fish expressing Chr2 in sensory afferents. Top trace shows responses of the MC to 12 repetitions of the stimulus sequence; bottom trace shows averaged membrane potential after removing spikes by median filtering. The approximate location of the recorded MC relative to the squares is shown in the map (oval outline approximates the OB). Black traces at the location of each square show the mean membrane potential change upon optical stimulation (blue ticks; red: zero line). The sequence of activation of the squares is shown on the right. Depolarizations of approximately 10 mV and spiking was evoked by activating squares near the recorded MC. **b**, Responses of the same cell to optical stimulation with 20 x 20 µm^2 squares (22 repetitions; corresponding to stimulus set 2). Depolarizations of approximately 5 mV and spiking is seen when squares near the cell are activated. **c**, Responses of the same cell to the activation of single mirrors (0.67 x 0.67 µm^2) at the center of each 20 x 20 µm^2 square (9 repetitions). No obvious response is detectable. Similar results have been obtained in two fish. This example was chosen because the MC showed low spontaneous activity, simplifying the recognition of stimulus-evoked spikes.

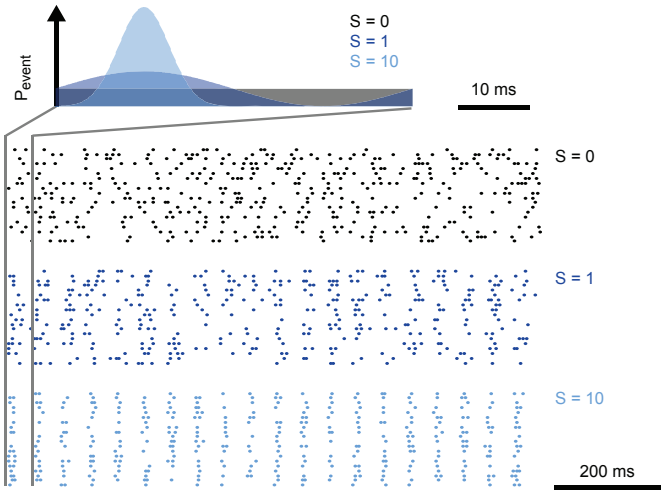

Supplementary Figure 4 | Oscillatory modulation of synchrony in trains of events. Top: probability density functions used to generate trains of events with different synchrony *S*. At $S = 0$, the instantaneous probability of an event is constant. At $S > 0$, the probability is periodically modulated at a carrier frequency of 20 Hz by drawing individual events from probability distribution $P(t)$ given by

$$P(t) = X(t) / \int_0^{tmax} X(t)\, dt$$

with

$$X(t) = (S \times \sin(20 \times 2\pi \times t) + 1) \qquad | S \leq 1$$

$$X(t) = (\sin(20 \times 2\pi \times t) + 1)^S \qquad | S > 1$$

where $t \leq t_{max}$ is time in seconds and *S* is the synchronization index . To allow for a refractory period, events closer than 5 ms were forebidden. Modulation increases with *S* but the time-averaged probability of events remains constant. See Methods for more details. Bottom: examples of event train patterns.

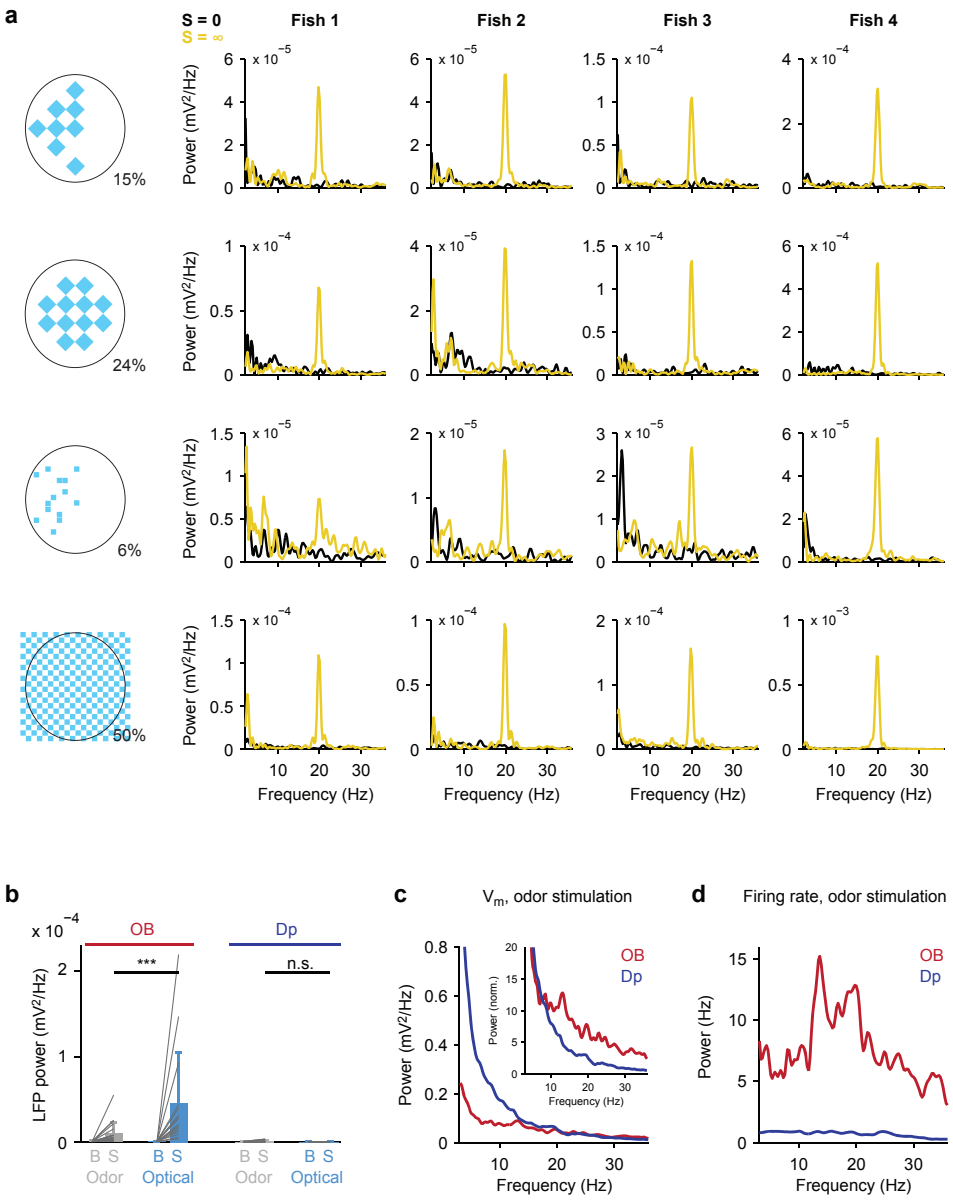

Supplementary Figure 5 | Additional power spectral analyses. **a**, Power spectra of LFP recordings in the OB of four individual fish (columns) in response to four different optical stimulus patterns (left). Each stimulus was presented at $S = 0$ (no synchrony; black) and $S = \infty$ (high synchrony; yellow). Power spectra show that all stimuli evoked prominent 20 Hz LFP oscillations in all OBs when presented at $S = \infty$, but not at $S = 0$. **b**, Mean LFP power (± s.d.) evoked by five odor stimuli (food extract, three individual amino acids and mixture; 10 µM or 100 µM) and four optical stimulus patterns at high synchrony ($S = \infty$) in the OB (left) and Dp (right). LFPs in the OB and Dp were measured simultaneously in the same fish ($n = 4$ fish). B: power of baseline LFP before stimulus onset; S: power during stimulus. Lines show changes in LFP power for individual stimulus-fish pairs. In odor trials, power was measured in a 4 Hz frequency band centered on the peak frequency between 10 and 30 Hz. In experiments using optical stimulation, power was measured in a 4 Hz frequency band centered on 20 Hz. In the OB, optical stimuli evoked significantly stronger LFP responses than odor stimulation ($P < 0.001$). No substantial LFP oscillation was observed in Dp in response to optical or odor stimulation, and power during optical and odor stimulation was not significantly different ($P = 0.22$). ***, $P < 0.001$; "n.s.", not significant. **c**, Power spectra of membrane potential fluctuations during odor stimulation in MCs and Dp neurons. Power spectra were calculated for each trial and averaged over trials and stimuli. Inset shows power spectra normalized to the total power between 0 and 500 Hz. The power spectrum of Dp neurons decays gradually, similar to the passive filter function of Dp neurons (Fig. 4b). The power spectrum of MCs is more complex and has a broad shoulder in the oscillatory frequency range. **d**, Power spectra of firing rates of MCs and Dp neurons during odor stimulation. Power spectra were calculated for each trial and averaged over trials and stimuli. The mean power spectrum of MCs, but not that of Dp neurons, shows a complex peak in the oscillatory frequency range.

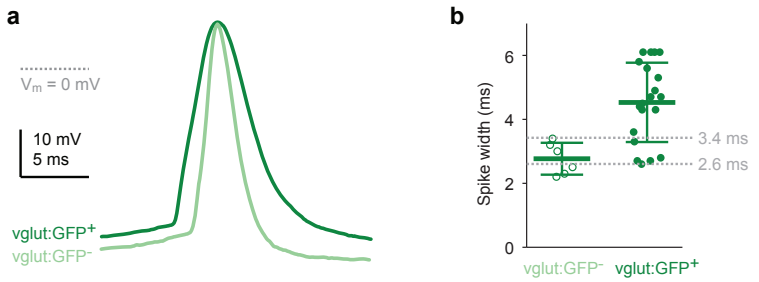

Supplementary Figure 6 | Coarse classification of neuron types by spike width. **a**, Spikes recorded from a GFP-positive neuron and a GFP-negative neuron in fish expressing GFP under the control of the promoter of the vesicular glutamate transporter 2a. **b**, Spike widths of GFP-positive and GFP-negative neurons. Horizontal lines and error bars show mean ± s.d..

To obtain insights into the types of neurons recorded in optical and odor stimulation experiments, we performed whole-cell recordings in transgenic fish expressing GFP from the promoter of the vesicular glutamate transporter 2a, a marker for glutamatergic neurons[2]. We evoked action potentials by current injection and compared their waveforms between GFP-positive neurons ($n = 20$) and GFP-negative neurons ($n = 6$). GFP-positive neurons had significantly broader action potentials, as quantified by the width at half height (4.5 ± 1.2 ms vs. 2.8 ± 0.5 ms; $P < 0.01$). None of the GFP-negative neurons had a spike width >3.4 ms, and none of the GFP-positive neurons had a spike width <2.6 ms. We then measured the width of spikes evoked by current injection in 53 neurons from fish that did not express vglut2a:GFP. These included 34 neurons from Chr2-transgenic fish used for optical stimulation experiments and 19 neurons from wild-type fish used for odor stimulation experiments. 18 of these neurons (34 %) had a spike width >3.4 ms, and 20 neurons (38 %) had a spike width <2.6 ms. Neurons recorded in experiments using optical or odor stimulation therefore probably included both principal neurons and interneurons.

2 Miyasaka, N. *et al.* From the olfactory bulb to higher brain centers: genetic visualization of secondary olfactory pathways in zebrafish. *J. Neurosci.* **29**, 4756-4767 (2009).

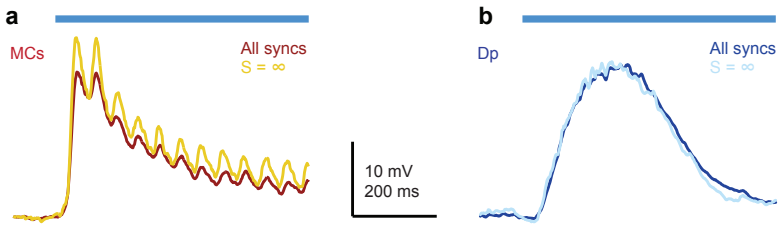

Supplementary Figure 7 | Selective analysis of large responses to optical stimulation. **a**, Average membrane potential time course of the 10 % largest MC responses to optical stimulation (red; $n = 64$ responses), and the 10 % largest responses to stimuli with $S = \infty$ only (yellow; $n = 16$ responses). **b**, Same analysis for Dp neurons ($n = 37$ responses and $n = 9$ responses).

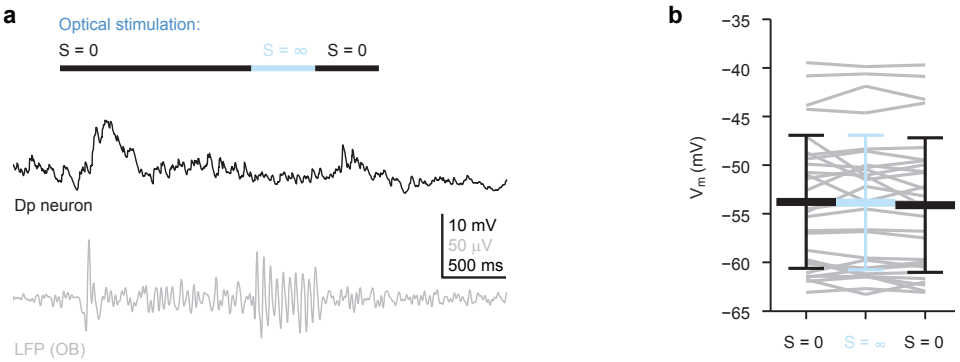

Supplementary Figure 8 | Switching synchrony does not evoke responses. **a**, Black trace: response of a Dp neuron (whole-cell recording) to an optical stimulus (2.5 s duration) that included a sudden switch in synchrony from $S = 0$ to $S = \infty$ at 1.5 s after stimulus onset and back to $S = 0$ at 2 s (average over four repetitions). Gray trace: simultaneously measured LFP in the OB. **b**, Mean membrane potential averaged over 500 ms immediately before the switch in synchrony ($S = 0$), after the swich to high synchrony ($S = \infty$), and after switching back to $S = 0$. Each gray line shows the change in mean membrane potential for one stimulus-neuron pair ($n = 28$ stimulus-neuron pairs in 14 Dp neurons). Thick lines and error bars show mean ± s.d.. No significant change in membrane potential is observed upon switching to $S = \infty$ ($P = 0.63$; paired sign test) and back ($P = 0.14$; paired sign test).

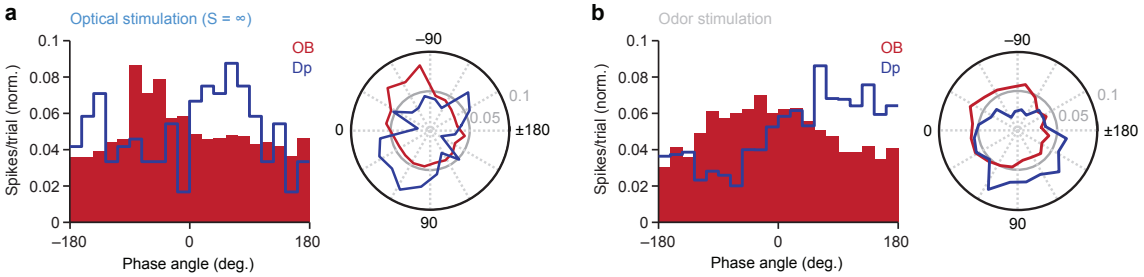

Supplementary Figure 9 | Analysis of spike phase relative to the LFP oscillation in the OB. **a**, Red: phase distribution of MC spikes evoked by optical stimulation with high synchrony ($S = \infty$) relative to the simultaneously recorded LFP oscillation in the OB ($n = 1430$ spikes). Zero degrees corresponds to the positive peak of the LFP. MC spikes occured preferentially shortly before the positive peak. Blue: same analysis for simultaneous recordings of Dp neurons and LFP oscillations in the OB ($n = 120$ spikes). Spikes in Dp occurred more frequently after the peak of the LFP. Right: same histogram as polar plot. Both spike phase distributions were significantly different from a uniform distribution (Raleigh test, $P < 0.025$) and from each other (Kuiper's test, $P < 0.001$). **b**, Same analysis for spikes evoked by odor stimulation (MCs: $n = 2908$ spikes; Dp: $n = 350$ spikes). Both spike phase distributions were significantly different from a uniform distribution (Raleigh test, $P < 10^{-10}$) and from each other (Kuiper's test, $P < 0.001$).

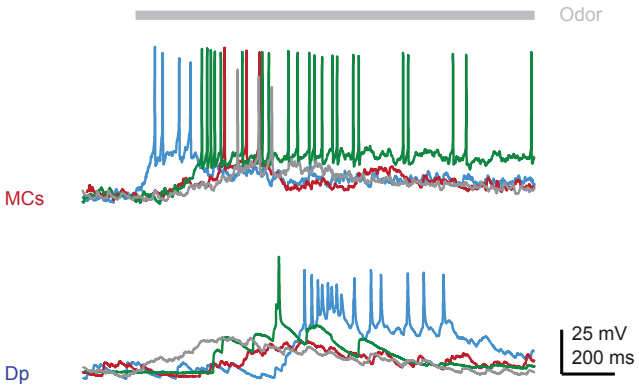

Supplementary Figure 10 | Examples of odor responses of mitral cells and Dp neurons. Responses of four MCs (top) and four Dp neurons (bottom) to odor stimulation (gray bar).

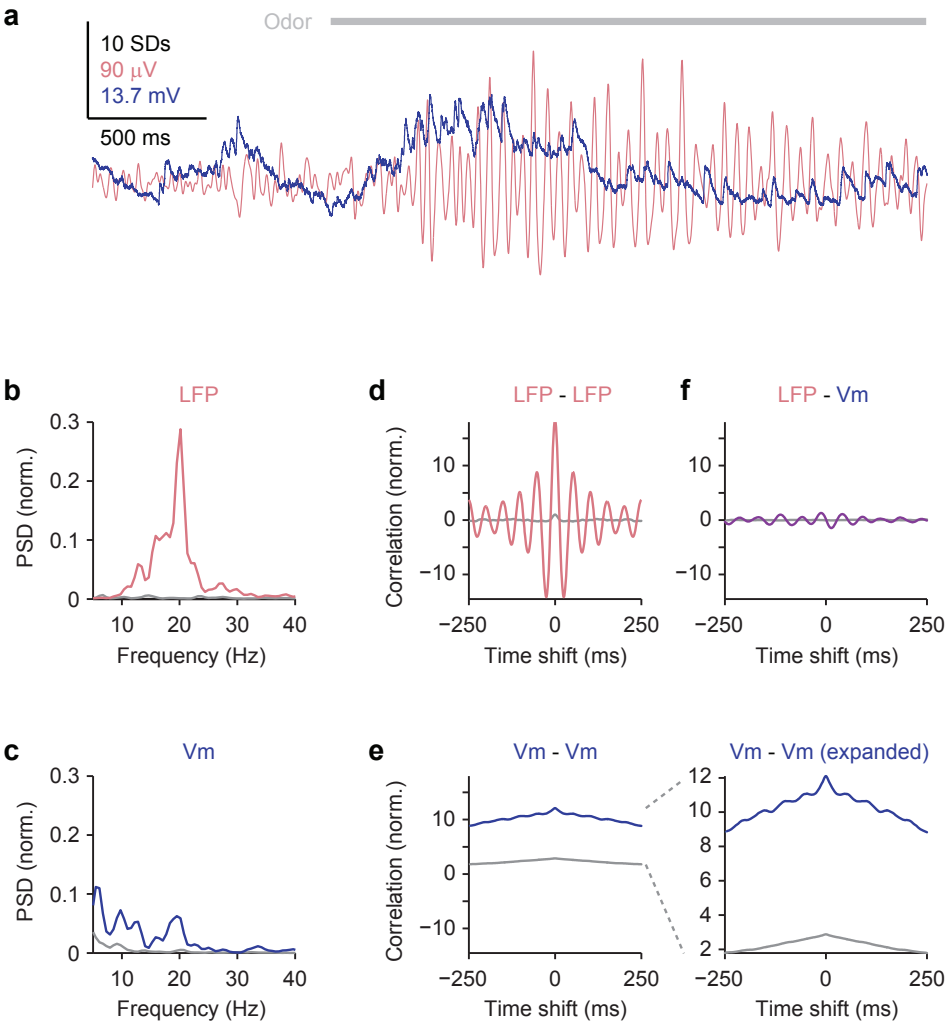

Supplementary Figure 11 | Correlation between LFP oscillation in the OB and membrane potential fluctuations of a Dp neuron during an odor response. **a**, LFP (red; 5 – 40 Hz) and membrane potential of a simultaneously recorded Dp neuron (blue) during odor stimulation (gray bar). Each trace was normalized by its s.d.. Normalized traces were used for all further analyses presented in this figure to allow for the comparison of LFP and membrane potential data on similar scales. Same experiment as in Fig. 3a. **b**, Power spectrum of normalized LFP before (gray) and after (red) onset of the odor response. **c**, Power spectrum of normalized membrane potential trace before (gray) and after (blue) onset of the odor response. **d**, Autocorrelation of normalized LFP before (gray) and during (red) odor stimulation. **e**, Autocorrelation of normalized membrane potential trace before (gray) and during (blue) odor stimulation. Note that the oscillatory modulation of the autocorrelation function is small relative to the slow component. **f**, Cross-correlation of LFP and membrane potential.

This example was selected because it showed more pronounced oscillatory modulations of auto- and crosscorrelation functions than most other responses. Nevertheless, correlated oscillatory membrane potential fluctuations were small compared to the slow depolarization, which is evident in the raw traces (**a**), the power spectrum (**c**), and the auto- and crosscorrelations (**e, f**).

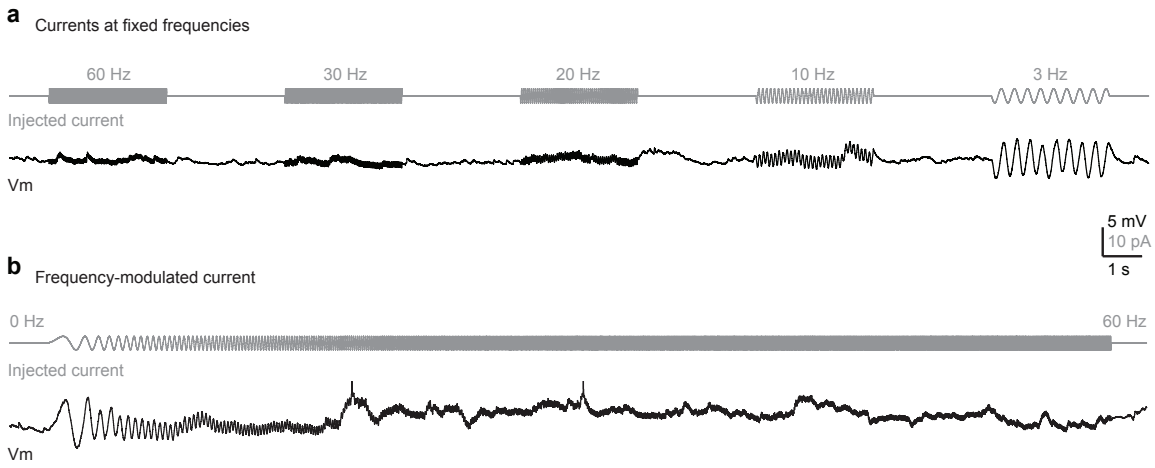

Supplementary Figure 12 | Resonance properties of Dp neurons. **a**, Response of a Dp neuron to injection of sinusoidal currents at fixed frequencies (3, 10, 20, 30, 60 Hz). Gray: injected current. Black: membrane potential. **b**, Response of a Dp neuron to injection of a frequency-modulated sinusoidal current. Gray: injected current. Black: membrane potential. Two action potentials were clipped. In each neuron, two trials with frequency modulations in opposite directions were recorded, and results were averaged. Amplitudes of fixed-frequency and frequency-modulated currents were adjusted to depolarize neurons close to, but usually below, spike threshold.

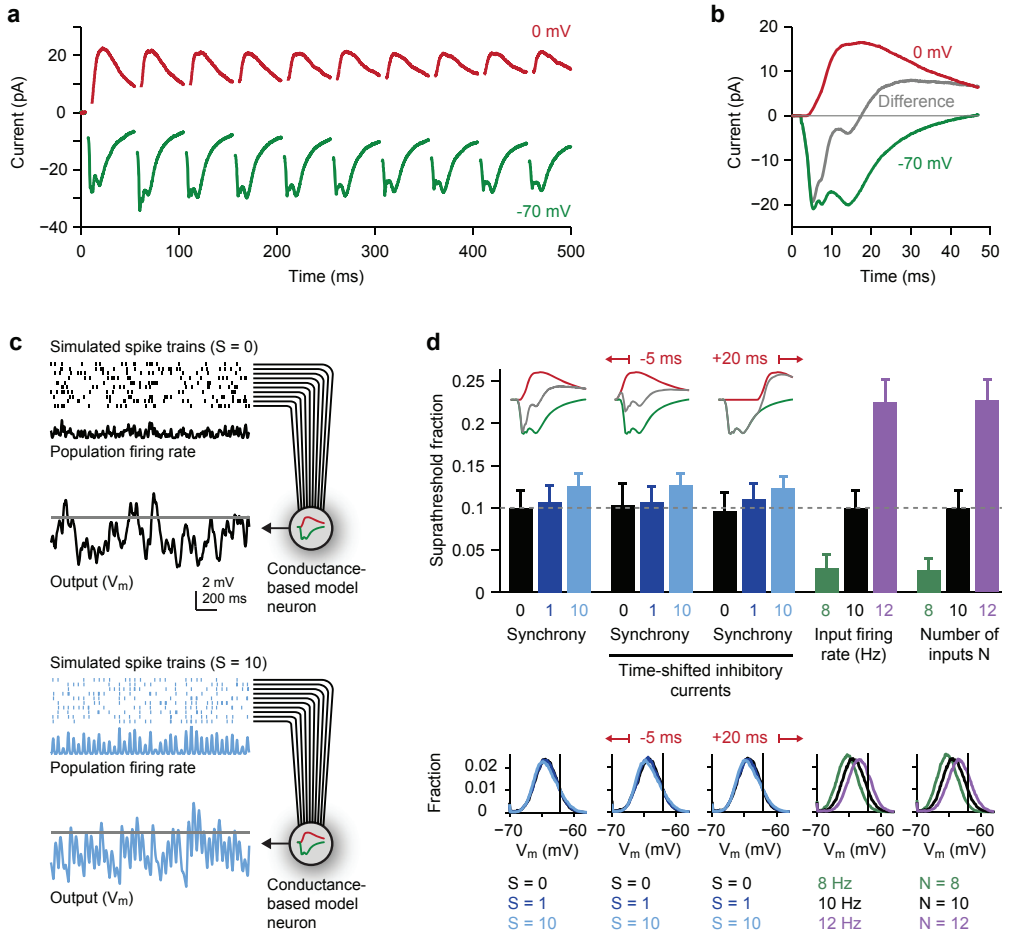

Supplementary Figure 13 | Analysis of synchrony detection by delayed inhibition using a conductance-based model neuron. **a**, Mean excitatory (green) and inhibitory (red) currents evoked by electrical stimulation of the olfactory tract (10 pulses; 20 Hz) in Dp neurons (n = 30 from 12 fish). Excitatory and inhibitory currents were recorded in voltage clamp at holding potentials of -70 mV and 0 or -10 mV, respectively. Stimulus artifacts are blanked out. **b**, Baseline-subtracted currents averaged over the first five stimulus cycles. **c**, Simulation of the membrane potential evolution in a passive conductance-based model neuron in response to input spike patterns of $N = 10$ simulated neurons with synchrony $S = 0$ and $S = 10$. Each spike evoked excitatory and inhibitory currents in the model neuron with waveforms given by the measured currents shown in **b** (extrapolated to 250 ms). The amplitude of the current evoked by an individual input was the measured current divided by $N = 10$. Gray line shows threshold to detect 10 % of the membrane potential values as suprathreshold in response to input spike patterns with $S = 0$. **d**, Top: suprathreshold membrane potential fraction of the model neuron in response to spike patterns with different synchrony, different timing of currents, different mean firing rate, or different numbers of inputs. Insets show excitatory and inhibitory currents without time shift (left; same as **b**; only first 50 ms shown) and time-shifted inhibitory currents. Bottom: membrane potential distribution of the model neuron under the different conditions. Vertical line shows threshold.

In many brain areas, excitatory input to principal neurons is followed a few milliseconds later by polysynaptic inhibition[3], resulting in a narrow time window for synaptic integration that favors the detection of coincident input. For efficient detection of oscillatory input by such microcircuits, membrane time constants and synaptic currents have to be short relative to the oscillation period. Otherwise, input would summate over cycles and approach a steady-state, rather than undergo a periodic reset in each cycle. Coincidence detection by delayed inhibition therefore depends on the intrinsic properties of target neurons and on the time course of synaptic currents. To examine these effects in Dp neurons, we first recorded excitatory and inhibitory synaptic currents evoked by 20 Hz electrical stimulation of small fiber bundles in the olfactory tract, which contains projecting MC axons (**a, b**; $n = 30$ neurons from 12 fish). Current responses frequently contained multiple components with different latencies. Currents with short latencies (<5 ms) were exclusively excitatory and most likely represent monosynaptic MC input. The mean excitatory current showed multiple peaks, with later peaks presumably reflecting multisynaptic input from neurons in Dp or other brain areas (**a, b**). The mean inhibitory current was delayed by approximately 5 ms, did not show distinct peaks, and decayed more slowly. Inhibitory currents were frequently observed in the absence of short-latency excitatory currents in the same cell (not shown). Hence, Dp neurons receive direct and indirect excitation, as well as strong polysynaptic inhibition that appears to be widespread. These results are consistent with observations in mammalian olfactory cortex[4-7] and show that delayed polysynaptic inhibition is present in Dp.

To examine the consequences for oscillatory input we simulated a conductance-based target neuron with passive properties similar to those of Dp neurons. The target neuron received $N = 10$ inputs, each firing at a mean rate of 10 Hz (**c**). Each input spike produced excitatory (reversal potential $V_{rev, exc} = 0$ mV) and inhibitory ($V_{rev, inh} = -70$ mV) input currents with latencies and time courses given by the measured currents. Synchrony among inputs was varied by varying the synchronization index S (Supplementary Fig. 4). A threshold was then defined that classified the membrane potential as suprathreshold for 10 % of the time in response to unsynchronized input ($S = 0$). Increasing synchrony increased the suprathreshold fraction of the membrane potential only slightly (**d**). To examine whether this effect depended on delayed inhibition, we reduced the latency of inhibitory currents by 5 ms to decrease the integration time window, or we increased the latency by 20 ms to extend the integration time window. In both cases, the dependence of the suprathreshold membrane potential fraction on synchrony was nearly unchanged (**d**), demonstrating that the relative timing of inhibition and excitation does not select synchronized input. Modest changes in the number or the mean firing frequency of active inputs, in contrast, substantially changed the suprathreshold membrane potential fraction (**d**). Hence, delayed feed-forward inhibition did not effectively detect synchronized input because passive membrane properties act as strong low-pass filters (see also Fig. 4b), and because inhibitory synaptic currents are slow.

3 Pouille, F. & Scanziani, M. Enforcement of temporal fidelity in pyramidal cells by somatic feed-forward inhibition. *Science* **293**, 1159-1163 (2001).

4 Poo, C. & Isaacson, J. S. Odor representations in olfactory cortex: "sparse" coding, global inhibition, and oscillations. *Neuron* **62**, 850-861 (2009).

5 Franks, K. M. & Isaacson, J. S. Strong single-fiber sensory inputs to olfactory cortex: implications for olfactory coding. *Neuron* **49**, 357-363 (2006).

6 Luna, V. M. & Schoppa, N. E. GABAergic circuits control input-spike coupling in the piriform cortex. *J. Neurosci.* **28**, 8851-8859 (2008).

7 Stokes, C. C. & Isaacson, J. S. From dendrite to soma: dynamic routing of inhibition by complementary interneuron microcircuits in olfactory cortex. *Neuron* **67**, 452-465 (2010).

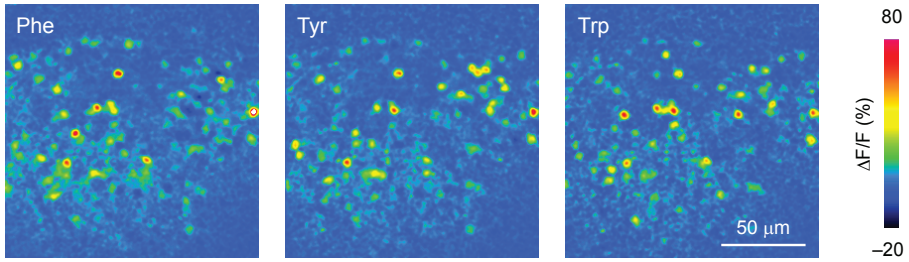

Supplementary Figure 14 | Multiphoton calcium imaging of odor response patterns in Dp. Time-averaged patterns of calcium signals evoked by three similar odors (Phe, Tyr, Trp; 10 μM) in Dp, measured by 2-photon calcium imaging.

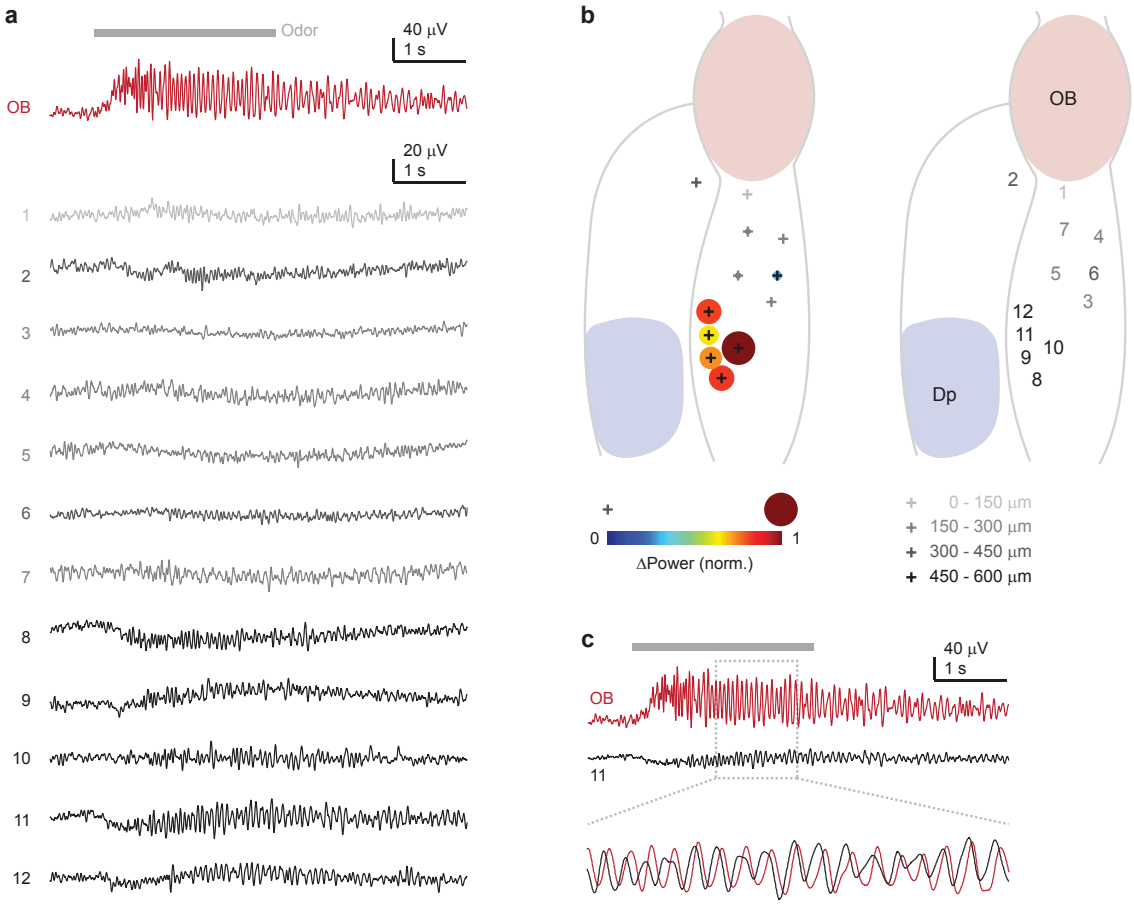

Supplementary Figure 15 | Oscillatory LFP responses to odor stimulation in different telencephalic areas. **a**, LFP recordings (5 – 40 Hz) evoked by odor stimulation (food extract) in the OB (red) and at 12 different locations in the telencephalon outside Dp. **b**, Map showing the approximate position of recording sites (location of pipette tip) relative to the outline of the telencephalon (ventral view). Each recording site is indicated by a cross; corresponding numbers are shown on the right. Gray levels indicate depth of recording sites (from ventral to dorsal) relative to the ventral surface of the telencephalon near the anterior commissure. Left: size and color of circles show the mean increase in LFP power during an odor response relative to the pre-odor period, normalized to the maximum power change observed in the telencephalon (average over 2 – 3 trials at each location). Power was measured in a 4 Hz band centered on the peak frequency of the oscillation in the OB. Large oscillatory LFP responses occurred in a deep region close to the center of the telencephalon. This region is near subpallial areas Vs and Vd, which are related to striatal areas in mammals. **c**. Simultaneous recordings of LFP oscillations in the OB and at location 11. Expanded and normalized traces (bottom) show phase-locking of LFP oscillations. Similar results were obtained in 4 fish.